Ralstonia pseudosolanacearum LOV domain protein regulates environmental stress tolerance, iron homeostasis, and bacterial wilt virulence

Bridget S. O'Banion*[1], Mariama D. Carter*[1a], José A. Sanchez Gallego[1], Hanlei Li[1], Stephanie S. Hayes[1], Marlee Strysick[1], Ja'Nyla Holcomb[2], Caitilyn Allen[#1]

[1] Department of Plant Pathology, University of Wisconsin-Madison, Madison, USA

[2] Department of Agricultural Science and Engineering, Tennessee State University, Nashville, USA

[a]Current address: Crop Genetics Department, John Innes Centre, Norwich Research Park, Norwich, UK

*Contributed equally to this work

[#]Corresponding author; callen@wisc.edu +1 608-556-3369

Keywords: LOV protein, microbial stress regulation, host-bacteria interactions, bacterial wilt, *Ralstonia pseudosolanacearum*, plant pathology

Author contributions. Research conceptualization and experimental design: BSO, MDC, JASG, and CA; experimentation and data analysis: BSO, MDC, JASG, HL, SH, MS, and J'NH; writing manuscript: BSO and MDC; editing manuscript: BSO, MDC, and CA.

Funding: This project was supported by a National Science Foundation Graduate Research Fellowship DGE-1747503 to MDC, a USDA Hatch project WIS04091 to CA, and the University of Wisconsin-Madison College of Agricultural and Life Sciences. Any opinion, findings, and conclusions or recommendations expressed in this material are those of the authors and do not necessarily reflect the views of the National Science Foundation.

Abstract

Bacteria use diverse sensors to integrate environmental stimuli into physiological responses that ensure fitness and survival. *Ralstonia pseudosolanacearum* (*Rps*), a soil-borne plant pathogen that causes bacterial wilt disease, encodes a conserved LOV (light-oxygen-voltage) protein that mediates photoreception across the tree of life. However, *Rps* had a minimal LOV-dependent transcriptional response to light in culture. Clues from functional domains, the *lov* genomic neighborhood, and transcriptional analyses suggest that LOV shapes *Rps* biology in response to stress. Loss of LOV did not affect *Rps* biofilm or motility *in vitro*, but did influence expression of genes encoding for these phenotypes *in planta*. The Δ*lov* mutant had reduced heat tolerance and broad metabolic dysregulation, leading to growth defects on several carbon sources but a growth advantage in *ex vivo* tomato xylem sap and in high-iron medium. *In vitro*, the Δ*lov* mutant was more tolerant than wild type of redox stress and the antimicrobial phenolic caffeate, but *Rps* required *lov* for full virulence on tomato. LOV mediated attachment to the root surface, stem colonization, and overall symptom development. Together these findings reveal that LOV, which is highly conserved among plant pathogenic *Ralstonia*, modulates *Rps* stress response and virulence independently of light cues, but in a plant-dependent fashion.

Importance

Like other plant-associated microbes, the destructive crop pathogen *Ralstonia pseudosolanacearum* (*Rps*) must integrate a complex array of biotic and abiotic signals to successfully infect and colonize the roots and xylem vessels of its plant hosts. *Rps* encodes a large LOV domain protein. LOV proteins sense blue light in leaf colonizing microbes, but *Rps* inhabits soil, plant roots, and xylem where there is little blue light. Although deleting *lov* had only minor effects when the bacterium grew in culture, many genes were dysregulated when the Δ*lov* mutant infected tomato plants. Functional experiments showed LOV has diverse light-independent roles in *Rps*, including modulating environmental stress tolerance and cellular iron and redox status. Most importantly, *Rps* needs LOV to grow normally in plants and cause bacterial wilt disease. Thus, LOV is a key sensor-regulator that controls *Rps* adaptation to the plant environment and virulence.

Introduction

The abundant organic carbon fixed by photosynthesis makes plants an attractively nutrient-rich habitat, but life with a plant can be stressful for bacteria (1). For example, *Ralstonia pseudosolanacearum* (*Rps*) must overcome high levels of oxidative stress, toxic phenolic compounds, and other defenses to infect plant vascular systems and cause bacterial wilt disease (2–8).

To manage plant-associated stresses, bacteria depend on sensors and regulators. Plant pathogenic *Ralstonia,* including *Rps,* have evolved a complex regulatory network with hundreds of players including cell surface receptors, secondary messengers, quorum sensing systems, and transcriptional activators (8–12). These intersecting signaling cascades help *Ralstonia* survive in soil and water, move toward and attach to host root surfaces, enter the root endosphere via wounds or natural openings, and locate the water-transporting xylem tissue (13–16). Once inside xylem vessels, the pathogen must adjust its metabolism to this specialized environment, attach to vessel walls, form biofilms, and spread systemically throughout the plant (9, 17–19). *Ralstonia* spp. are well adapted to plant xylem, rapidly growing to densities greater than 10^8 CFU/g stem. These large bacterial populations and their associated biofilm matrix fill xylem vessels and block water transport, leading to the characteristic wilting symptoms and death (20, 21). At each stage of this life cycle *Rps* must fine-tune its gene expression to succeed in the plant. Despite decades of research on these systems, many elements of this regulatory network remain unknown.

Diverse bacteria use flavin-binding LOV (light-oxygen-voltage) domain proteins to perceive and respond to signals such as blue light and reactive oxygen species (ROS) (22–24). Among other traits, LOV proteins regulate virulence in plant and human pathogens (25, 26). In plant-associated bacteria, photoreceptors play a role in anticipatory water stress response, attachment, EPS production, and nodule formation (22, 27, 28).

The genome of *Rps* model strain GMI1000 encodes a large LOV domain-containing protein (hereafter LOV) that also contains EAL and GGDEF domains that putatively mediate degradation and synthesis, respectively, of the ubiquitous intracellular secondary messenger bis-(3,5)-cyclic dimeric GMP (c-di-GMP) (29). While little is known about c-di-GMP signaling in *Ralstonia*, a recent study found a GGDEF domain-containing protein in *Rps* is required for conversion of two 2',3'-cGMP to one 2',3'-c-di-GMP, which influenced biofilm formation, motility, and virulence (30). Because these behaviors are all associated with bacterial wilt virulence (8), we hypothesized that *Rps* uses LOV to regulate gene expression during plant pathogenesis in response to an environmental signal. Previous transcriptomic analyses found that *lov* (*rsp0254*) is 1.68-fold (log2) up-regulated when *Rps* GMI1000 grew in wilt-susceptible tomato plants relative to when it grew in rich CPG medium (31). Many LOV proteins respond to blue light, but others respond to cellular redox state, temperature fluctuations, and potentially other stimuli (32–34). While *Rps* may encounter blue light while living in the xylem, it is known that *Rps* encounters redox stress during plant infection (3, 35, 36).

To better understand the biological role(s) of this putative receptor/signaling protein, we constructed an in-frame deletion mutant of *lov* in *Rps* GMI1000 (Δ*lov*). Transcriptional analyses found that while few genes were differentially expressed in Δ*lov* under dark conditions or in blue light *in vitro*, this mutant dysregulated dozens of genes *in planta*. Many of the differentially expressed genes are involved in virulence and stress responses. Consistent with this, a suite of *in vitro* assays revealed that *Rps* Δ*lov* had altered tolerance to plant-relevant environmental stresses. The Δ*lov* mutant also had abnormal metabolic behaviors consistent with a role in cellular iron homeostasis and catabolic capacity. Together these findings indicate that LOV, which is conserved across the *R. solanacearum* species complex, regulates a wide array of functions required for fitness during plant infection and pathogenesis.

116 **Results**

117 **The *lov* sequence and surrounding genomic region is highly conserved across the *Ralstonia* genus.**

118 LOV domains are ubiquitous, enabling blue light and oxidative stress sensing across prokaryotic
119 and eukaryotic kingdoms (37, 38). Following a description of LOV in *Rps* (39), we explored the
120 conservation of the *lov* sequence and the surrounding genomic region across the entire *Ralstonia* genus.
121 We compiled 111 non-redundant *Ralstonia* genomes, including representatives from *R. pickettii*, *R.*
122 *insidiosa*, *R. mannitolilytica*, and the four phylotypes in the *Ralstonia solanacearum* species complex
123 (RSSC) (Table S1). Using the RSSC phylotype I model strain *Rps* GMI1000 *lov* gene as a query, we
124 identified a putative *lov* homolog in 106 of the 111 genomes (>95% of genomes). A maximum
125 likelihood tree of these *lov* genes aligns with the phylogeny of the genus *Ralstonia*, consistent with
126 vertical inheritance from a common ancestral bacterium (Figure S1A).

127 The larger genomic context of *lov* could provide clues to its biological function. Analysis of 12
128 representative *Ralstonia* genomes indicates that the synteny of this genomic region is also highly
129 conserved (Figure S1B). All analyzed genomes contain many genes neighboring *lov* related to iron
130 metabolism (*fur2*, *feoAB,* and a siderophore-interacting protein), energy/redox sensing (*aer2*), and
131 reactive oxygen species (ROS) detoxification (*ahpC1* and *ahpF)* (Figure 1A, Figure S1B, and Table S2).
132 A smaller set of genes distinguish the plant-pathogenic RSSC from other *Ralstonia*. A c-di-GMP
133 synthetase (*rsp0253*) is unique to the RSSC, while a three-gene cluster containing an
134 alkylhydroperoxidase, an acetyltransferase, and an FMN-dependent NADH-azoreductase is present only
135 in non-RSSC genomes (Table S2). Further, a hemin transport and degradation gene (*rsp0243-44*) were
136 found only in RSSC phylotype I, IV, and a single phylotype II genome (Figure S1B). Because bacterial
137 genes can be spatially organized based on function, these results suggest *lov* may affect cellular redox
138 and/or iron homeostasis.

139 In addition to the LOV domain, which is a subset of the PAS sensory domain superfamily (40),
140 the *Ralstonia* LOV protein contains several other domains (Figure 1B). These include an extracellular
141 ligand-binding Cache domain, a predicted membrane-spanning HAMP domain, and two additional
142 cytoplasmic PAS folds. LOV also contains two domains related to the balance of c-di-GMP: EAL,
143 which degrades c-di-GMP, and GGDEF, which synthesizes the signal (29). The *Ralstonia* domain
144 architecture is unusual; many other LOV proteins are histidine kinases and typically contain fewer
145 additional signaling domains (33). We investigated the amino acid conservation in each of the seven
146 domains in the LOV protein across all 106 LOV-encoding *Ralstonia* genomes. The EAL, GGDEF, and
147 LOV domains were highly conserved while the lowest level of conservation was observed in the
148 periplasmic Cache domain (Figure 1B).

149 Across bacteria, archaea, and eukaryotes more than 57% of LOV domains have a conserved
150 cysteine residue that can form a light-induced flavin-cysteine adduct (23, 41, 42). This critical cysteine
151 (Cys672 in *Rps* GMI1000) is present in RSSC strains and in the opportunistic human pathogen *R.*
152 *mannitolilytica* SN83A39, but is notably absent from two non-pathogenic *Ralstonia* species (Figure 1C).
153 Together, these sequence analyses suggest that LOV is a signal transduction protein that acts by altering
154 intracellular concentrations of c-di-GMP based on environmental sensory cues.

155

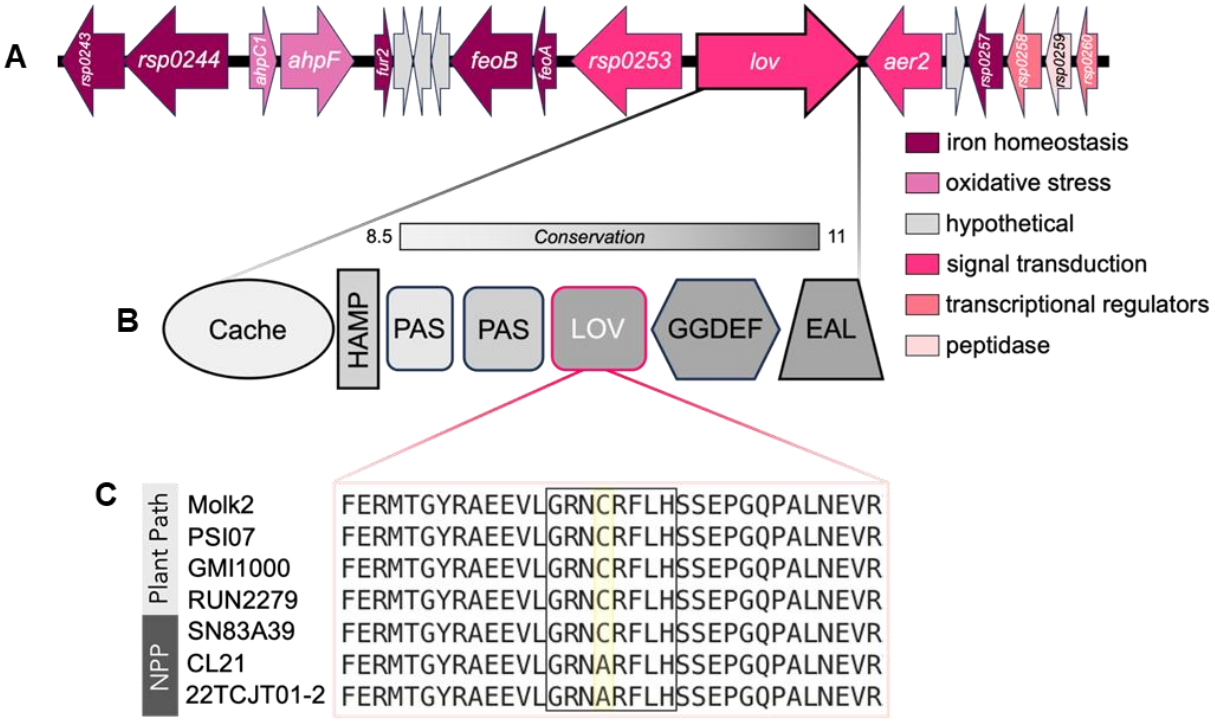

Figure 1: The multi-domain LOV protein and surrounding genes are conserved across the genus *Ralstonia*.

A) Genes surrounding *lov* (arrow with thicker border) on the *Rps* GMI1000 mega-plasmid. Arrow size represents approximate gene length. Gene arrows are color coded by functional category as indicated in upper right legend (see also Table S2) and manually visualized in the Joint Genome Institute Integrated Microbial Genomes web server (101). **B)** The domain architecture of the predicted LOV protein. Domains are labeled and represented as different shapes. Shading corresponds to average amino acid conservation (Shenkin conservation score, calculated with default parameters in Jalview (102)) within each domain boundary across 106 *Ralstonia* genomes (see also Table S1 and supplementary methods). The rounded rectangle labeled "LOV" denotes a PAS domain that encodes the characteristic LOV motif. **C)** Multiple-sequence alignment of a 34 amino acid region in the LOV domain. The comparison includes four representative RSSC strains (Plant Path) and three non-plant pathogenic (NPP) *Ralstonia* spp. The conserved 8 amino acid LOV motif is outlined by a black box. Yellow highlight indicates position 672 (GMI1000 as reference), which often encodes a highly conserved cysteine residue (Cys_{672}) where an oxidation-induced flavin-LOV adduct forms. The alignment was generated using Clustal Omega (accessed via EMBL-EBI web server) (103, 104).

Blue light affects expression of very few *Rps* genes *in vitro*.

We used RNA-seq to explore the global effects of *lov* and light in *Rps* GMI1000 and an in-frame *lov* deletion mutant (hereafter Δ*lov)*. We compared transcriptomes of Δ*lov* and wild-type GMI1000 *in vitro* in the presence and absence of blue light (Figure 2A). Strikingly, only three genes were differentially expressed at q ≤0.05 between the wild-type and Δ*lov* cells: *lov* itself (*rsp0254*), a hypothetical gene predicted to encode for a small peptide (*rsc1470*), and a universal stress protein (USP, *rsp1561*) (Table S3). These differentially expressed genes (DEGs) were down-regulated in Δ*lov*, and the hypothetical gene and USP were only differentially expressed between genotypes in dark conditions.

182 For a larger view of potential transcriptional effects, we expanded our analysis to include DEGs
183 with p ≤0.05. This larger set of genes included several involved in tolerance of reactive oxygen and
184 nitrogen species (*oxyR* and *norB*) and other stress response mechanisms (melanin production and
185 additional USPs) (Figure 2B, Table S3). Most of the less stringently defined DEGs, including those just
186 listed, were differentially expressed between genotypes in the dark (90 total genes) rather than under
187 blue light conditions (11 total genes). Further, only 85 genes were differentially expressed at p ≤0.05 in
188 wild-type cells exposed to dark vs. blue light, and none of these met the more stringent q-value cutoff.
189 Thus, blue light induces a minimal transcriptional change in *Rps* and *lov* may influence expression of
190 *Rps* stress response genes.

191

192 **LOV influences *in planta* transcription of *Rps* genes involved in host-relevant behaviors.**

193 Measuring *Rps* transcription *in vitro* identified very few DEGs. To assess the role of *lov* in a
194 more biologically relevant environment, we characterized *lov*-dependent transcription *in planta* (Figure
195 2A). Wild-type and Δ*lov Rps* were directly inoculated into susceptible tomato stems via a cut leaf petiole
196 and allowed to colonize the host for 3 days. RNA was extracted from stems containing similar
197 populations of wild-type (1.75-7.69x10^8 CFU/g) and Δ*lov* (1.50-7.56x10^8 CFU/g) cells, allowing direct
198 comparison of their transcriptional patterns.

199 A larger set of *Rps* genes were differentially expressed in the Δ*lov* mutant *in planta* than in
200 culture, including genes for many virulence traits. At the stringent q ≤0.05 cutoff, expression of five
201 genes decreased and nine genes increased in the Δ*lov* mutant. Using a p ≤0.05 cutoff identified 31 down-
202 regulated and 156 up-regulated genes in Δ*lov* (Figure 2C, Table S4). Loss of *lov* increased expression of
203 genes involved in general stress response (*rpoS*, USP [*rsp1561*]), degradation of phenolics (*fca*, *fcs,*
204 *pcaJ, pcaG*), attachment (*radA*, *lecX*, *tadG2*), and motility (*fliC, flgE, pilE2*). Genes involved in
205 glutathione metabolism (*rsp0532, rsc0788*), nutrient transport and metabolism (*exaC, eutBC, narG,*
206 *dctA1*), and c-di-GMP modulation (*rsc3143*, *rsp1623*) had variable expression patterns between the
207 bacterial genotypes, with some increased and some decreased in Δ*lov*. Expression of the entire
208 exopolysaccharide (EPS) biosynthesis cluster (*epsABCDEFP)* increased in Δ*lov*, consistent with the
209 reduced expression of negative EPS regulator *epsR*.

210 The hypothetical protein gene *rsc1470,* which was downregulated in Δ*lov in vitro,* was not
211 significantly dysregulated *in planta*. USP *rsp1561* was differentially expressed in both conditions, but in
212 opposite directions: deleting *lov* decreased *rsp1561* transcript levels *in vitro* but increased them *in*
213 *planta*. This pattern was more broadly reflected in the expression of stress-related genes across the two
214 datasets (Figure 2B-C, yellow circles). Many stress response genes were downregulated *in vitro* in the
215 *lov* mutant but upregulated *in planta*, indicating that LOV is a context-dependent modulator of *Rps*
216 stress responses. Thus, *in vitro* experiments are likely of limited value in understanding its biological
217 function.

218 Together, the comparative genomic and transcriptomics analyses described above suggest that
219 *lov* is involved in environmental stress response, iron and nutrient homeostasis, sessile-motile lifestyle
220 decisions, and virulence. We used functional assays to evaluate the role of *lov* in these behaviors.
221 Because *in vitro* RNA-seq indicated that blue light does not significantly alter the *Rps* transcriptional
222 landscape, light cues were not further studied.

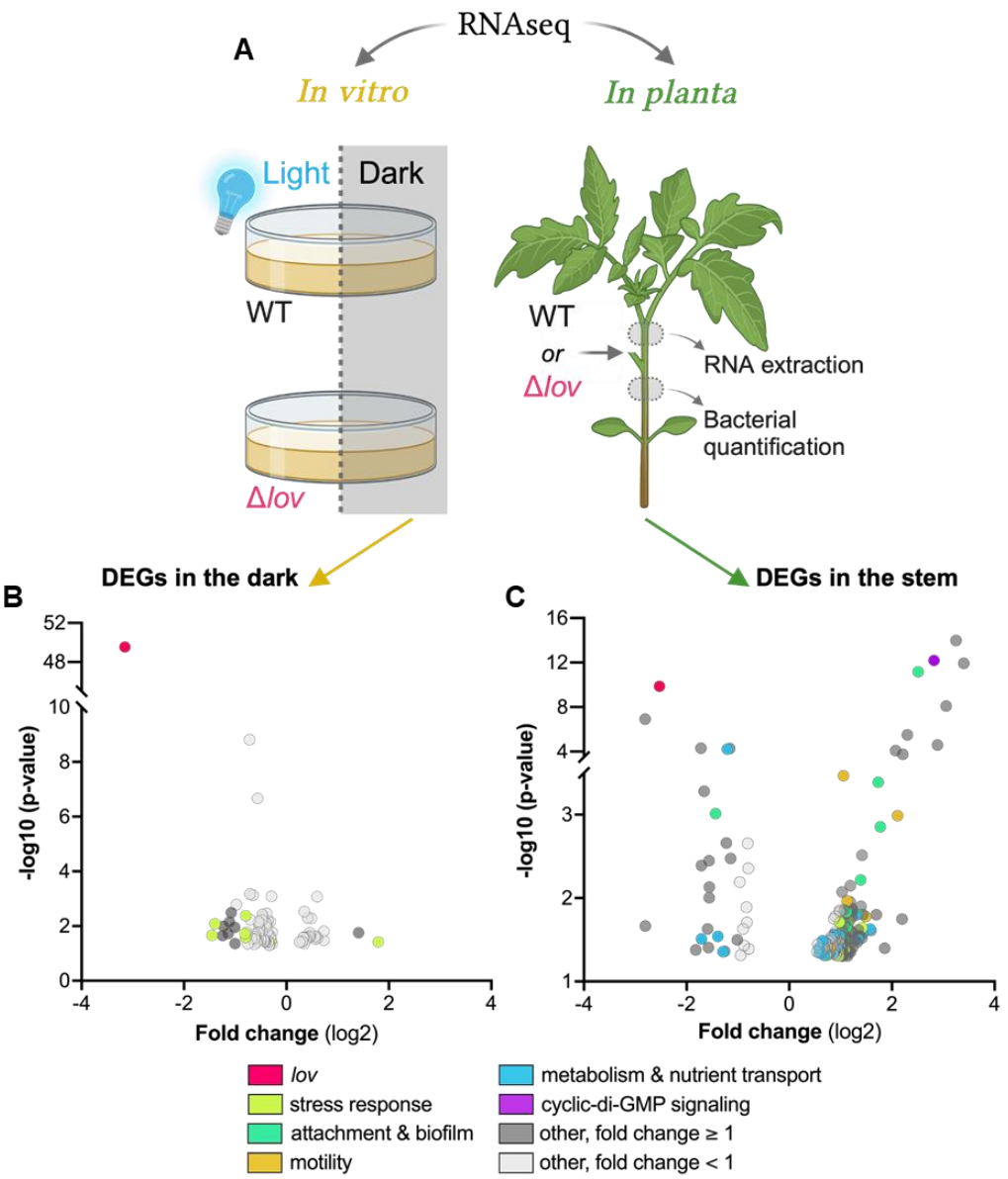

Figure 2: Mutating *lov* dysregulates *Rps* stress response and virulence gene expression *in planta.* A) Design of experiments comparing gene expression of *Rps* GMI1000 wild-type (WT) and Δ*lov*. **B-C)** Volcano plots showing differentially expressed genes (DEGs, P≤0.05) in Δ*lov* compared to wild-type *in vitro* (B) and *in planta* (C). Panel B shows DEGs in dark conditions. Each circle represents a single gene and is colored by functional categories shown in the legend. For genes that were not readily classified into listed categories, the corresponding circles are colored gray (light gray = log2 fold change < 1; dark gray = log2 fold change ≥ 1). Circles on the left of each graph represent genes with decreased expression in Δ*lov*; those on the right are increased in Δ*lov*. For a full gene list, see Tables S3 and S4.

236 **LOV mediates *Rps* responses to environmentally relevant stresses**

237 *In vitro* and *in planta* transcriptional analyses identified a USP as differentially expressed
238 between wild-type and Δ*lov* cells. USPs commonly regulate response to abiotic stressors such as UV,
239 redox, pH, toxins, and heat (43, 44). To test whether Δ*lov* had altered tolerance to abiotic stressors, we
240 first measured the mutant's response to high temperature. Heat is a relevant stress for *Rps*, which causes
241 disease in warm climates and the tropics (45). The Δ*lov* mutant had a slight reduction in growth
242 compared to wild-type at 28°C (Figure S2A). However, Δ*lov* grew ~30% less than wild-type at 37°C
243 (Figure 3A-B). This defect was observed in rich and minimal media (Figure S2B). Complementing Δ*lov*
244 with the wild-type *lov* gene under its native promoter (Δ*lov*+*lov)* partially restored this phenotype in
245 both media (Figures 3A-B and S2B). The phenotype was not restored by a version of *lov* with a single
246 missense mutation replacing the photoreactive cysteine residue with a non-reactive alanine
247 (Δ*lov*+lov_{C672A}). This indicated that chronic heat stress tolerance requires this reactive cysteine residue
248 (Figures 3A-B and S2B). We additionally investigated survival under acute UV irradiation and salt-
249 induced osmotic stress (27, 44). However, deleting *lov* did not change *Rps* response to either stress
250 under our experimental conditions (Figure S2C-D).

251 Plants often produce a ROS burst to restrict microbial growth, and a bacterium's ability to
252 detoxify oxidative radicals is important for successful plant colonization (46). We hypothesized that *lov*
253 plays a role in *Rps* oxidative stress response based on the conserved genes surrounding *lov* (*ahpC1*,
254 *ahpF*) and on hints from the transcriptomic analyses (*oxyR*, glutathione metabolism genes). Wild-type
255 and Δ*lov* cells were exposed to hydrogen peroxide (H_2O_2) to induce ROS stress. While the strains grew
256 similarly in the untreated control treatment, Δ*lov* recovered from H_2O_2 exposure and initiated
257 logarithmic growth ~3 hours before wild-type (Figure 3C), gaining a modest growth advantage (Figure
258 3D).

259 Plant-derived phenolic compounds can also induce oxidative stress (47). Deleting *lov* increased
260 *Rps* expression of *fcs* and *fca*, which encode the first two enzymes for the degradation of phenolic
261 hydroxycinnamic acids (HCAs) (4). We hypothesized Δ*lov* has increased tolerance to HCAs such as
262 caffeate, an antimicrobial HCA putatively involved in tomato resistance to bacterial wilt (48, 49). As
263 seen in response to H_2O_2, Δ*lov* grew better than wild-type in the presence of caffeate (Figure 3E-F and
264 S2E). Complementing Δ*lov* with Δ*lov*+*lov* partly restored wild-type growth in caffeate, but adding the
265 Δ*lov*+lov_{C672A} construct did not (Figure S2E). Though some comparisons were non-significant, this
266 result resembled the complementation pattern observed for the Δ*lov* heat tolerance phenotype (Figures
267 3B and S2B). Together, these assays validate a role for *lov* in modulating *Rps* response to high
268 temperature and some plant-relevant oxidative stresses.

269

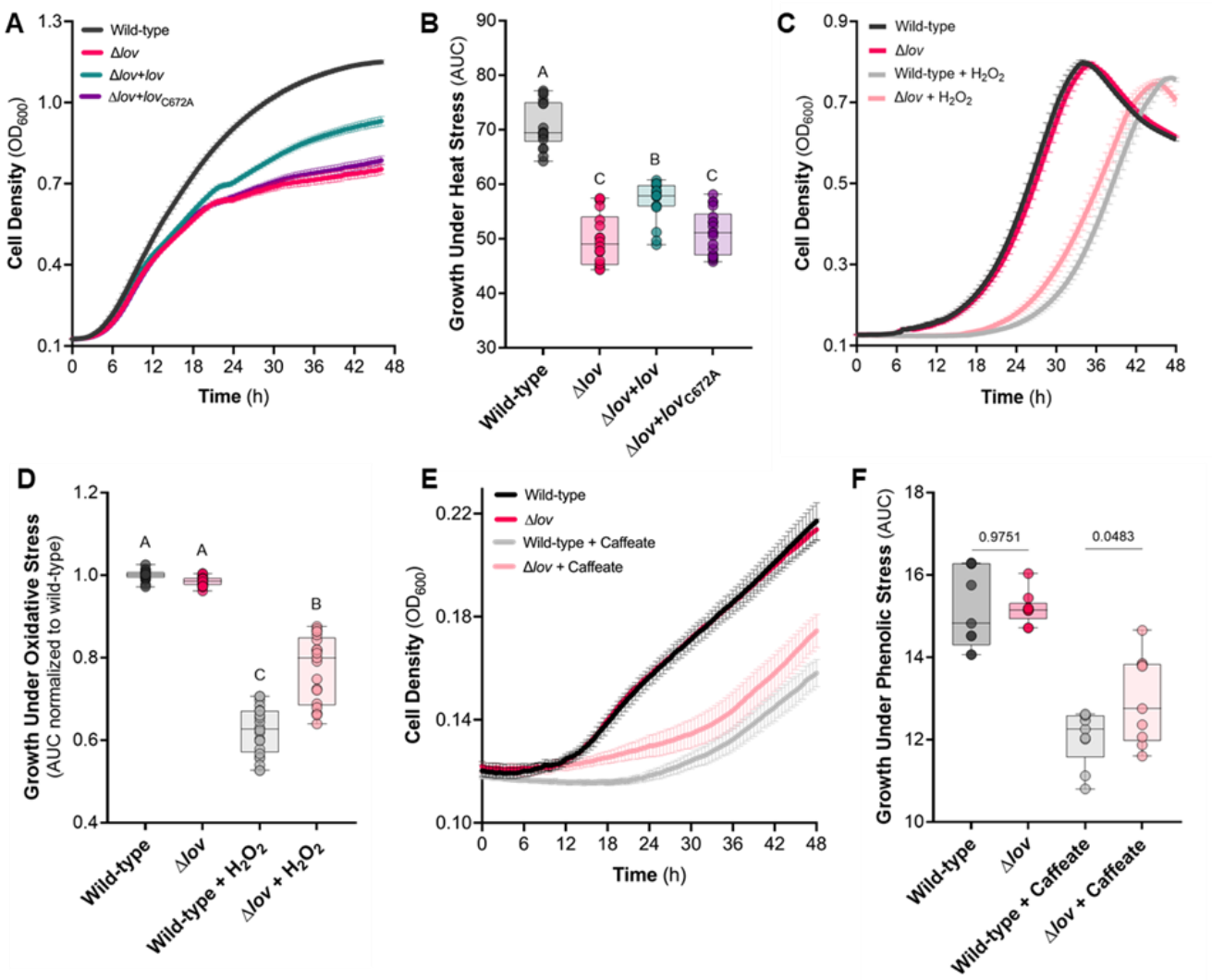

Figure 3: LOV modulates *Rps* abiotic stress tolerance. A-B) Growth of *Rps* strains in rich media at 37°C. Panel A error bars represent SEM. Data from panel A were used to calculate the area under the curve (AUC) in panel B, where each dot represents growth data for one microtiter well. Different letters indicate differences between groups ($P<0.05$, one-way ANOVA). The experiment was repeated 3 times with 6 technical replicates each (n=18 replicates per treatment). **C-D)** Growth of *Rps* strains in minimal media with and without 1.25 mM hydrogen peroxide (H_2O_2). Error bars in panel C indicate SEM. Data from panel C were used to calculate the AUC in panel D, where each dot represents growth data for one microtiter well. The AUC for each condition was normalized to that of the wild-type control without H_2O_2. Different letters signify differences between groups ($P<0.05$, one-way ANOVA). The data reflect three experiments with 3-12 technical replicates each (n=21-24 replicates per treatment). **E-F)** Growth of *Rps* strains in modified minimal media with and without 750 µM caffeate. Error bars in panel E represent the SEM. Data from panel E were used to calculate the AUC in panel F, where each dot represents growth data for one microtiter well (Welch's t-test). The experiment was repeated 3 times with 3 technical replicates each (n=9 replicates per treatment).

285

286 **Metabolism of *in planta* nutrients is influenced by LOV.**

287 Over its lifecycle *Rps* must obtain nutrients from oligotrophic environments including soil,
288 water, and xylem (8, 50). *In planta* transcriptomics suggested a connection between *lov* and genes
289 encoding nutrient transport and metabolism (Figure 2C). We therefore compared growth of wild-type
290 and Δ*lov* on nutrients known to be critical during pathogenesis.

291 Xylem sap fuels *Rps* multiplication in the pathogen's most explosive growth phase (17, 51).
292 Unexpectedly, the Δ*lov* mutant grew better than wild-type in *ex vivo* xylem sap from healthy tomato
293 plants (Figure 4A), indicating Δ*lov* can more effectively use some component(s) of healthy xylem sap in
294 this artificial condition. Because tomato sap is a carbon-limited environment (52), we compared the
295 metabolic fingerprints of wild-type and Δ*lov* on a panel of 31 carbon sources, including known sap
296 metabolites (Table S5). While many compounds in the panel contain both carbon and nitrogen (e.g.
297 glutamine and asparagine), our experimental design required their use as a sole carbon source. The wild-
298 type strain grew better than Δ*lov* on most tested carbon sources and no metabolite gave Δ*lov* a
299 significant advantage (Figure 4B and S3). A similar pattern was observed when we incorporated various
300 pH levels into the carbon use screen (Figure S4A-B, Table S6).

301 The *lov* genomic region is strikingly enriched in genes involved in regulation, transport, and use
302 of iron (Figure 1A). Iron is a closely guarded resource and iron-chelating siderophores are a common
303 bacterial virulence factor (53, 54). We measured siderophore activity in the cell-free supernatant of wild-
304 type and Δ*lov* cells grown in minimal media and found that Δ*lov* produces ~15% more siderophore-like
305 molecules than wild-type (Figure 4C). This increased siderophore production could provide a growth
306 advantage to Δ*lov* in medium with low levels (1x) of ferric iron – the target of siderophores. However,
307 the two strains grew similarly under ferric iron-limiting conditions (1x) (Figure 4D). On the other hand,
308 Δ*lov* grew significantly better than wild-type in medium containing higher levels (10x) of ferric iron
309 (Figure 4D). The Δ*lov* mutant maintained a growth advantage in the presence of very high levels (100x)
310 of both ferric and ferrous iron (Figure 4E-F). Ferrous iron is not targeted by siderophores and is instead
311 transported into the cell via the *feo* system, which is also encoded in the *Rps lov* gene cluster (Figure 1A)
312 (55). The growth advantage of Δ*lov* in ferrous iron indicates that its iron-dependent growth advantage is
313 not explained by its increased siderophore production. Rather, it suggests that LOV regulates cellular
314 iron homeostasis at multiple nodes of assimilation and utilization. Cumulatively, our nutrient assays
315 show that LOV helps *Rps* balance metabolism and growth in response to several different conditions.

316

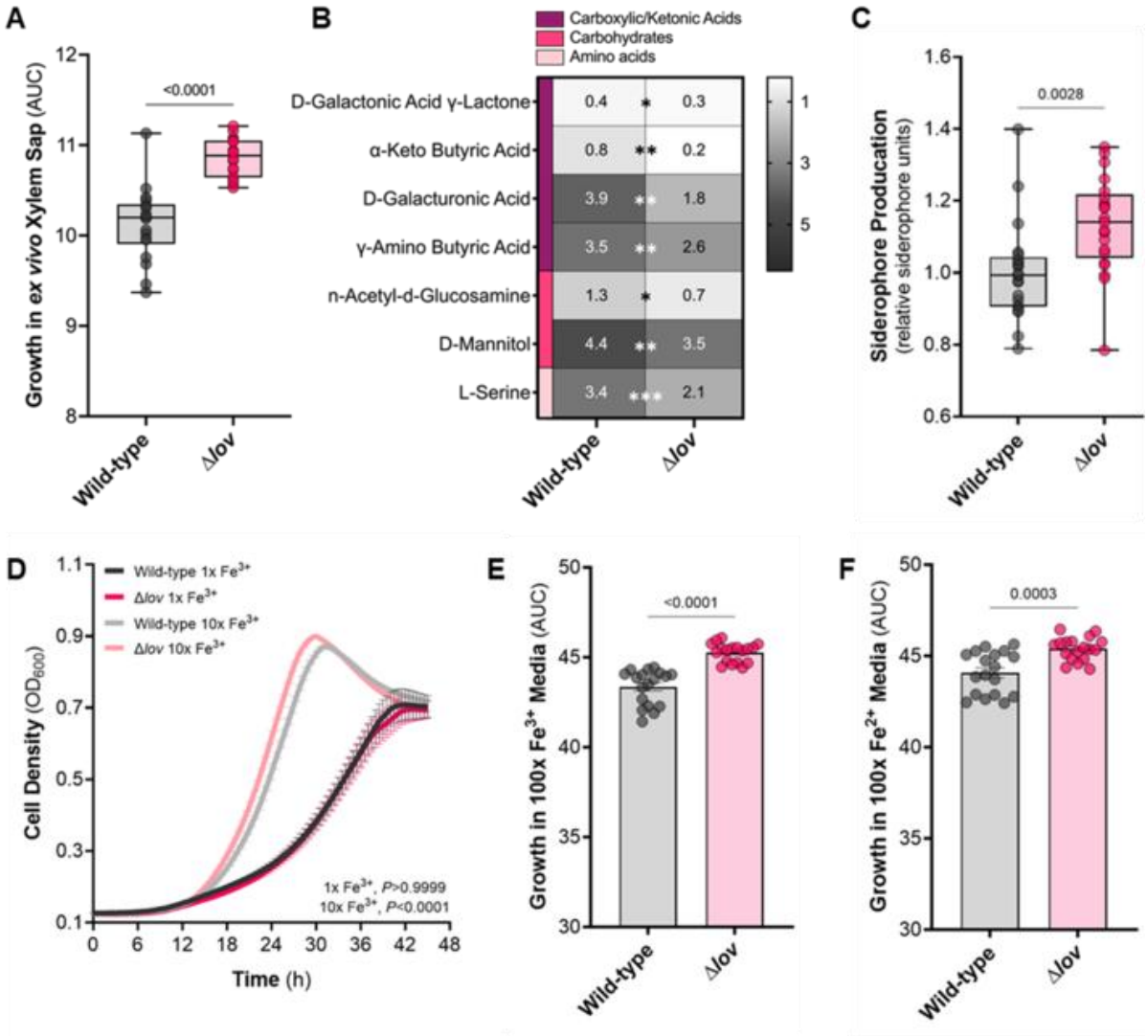

Figure 4: LOV influences metabolism and iron homeostasis in *Rps*. A) *Rps* growth in *ex vivo* xylem sap. Each circle represents the area under the growth curve (AUC) calculated for an individual microtiter well. Data shown represent 3 independent experiments, each with 6 technical replicates (n=18 per treatment, Welch's t-test). **B)** *Rps* growth in minimal media with different sole carbon sources. Grayscale shading indicates the average AUC across 3 biological replicates (n=9 wells per compound: 3 technical replicate wells per biologically distinct microtiter plate). The average AUC is also displayed in each box. Asterisks indicate a growth difference between the strains; more asterisks indicate a lower P-value (Student's t-test; * = P <0.05, ** = <0.01, *** = <0.001). Carbon sources are grouped and colored based on molecule type (see legend). Data shown in this panel are a subset of those shown in Figure S3 (also see Table S5). **C)** Relative production of siderophore-like molecules. Data are normalized to wild-type levels. Each circle represents a single microtiter well. Data represent 3 experiments, each with 7 technical replicates (n=21 per treatment, Mann-Whitney test). **D)** *Rps* growth in minimal media with 1x and 10x levels of ferric iron. Data represents 3 experiments with 8 technical replicates each (n=24 per treatment, RM two-way ANOVA). P-values above the x-axis indicate a comparison between wild-type and Δ*lov* within each treatment. Error bars indicate SEM. **E-F)** *Rps* growth in minimal media with 100x levels of ferric (E) or ferrous (F) iron. Each circle represents the AUC calculated for an individual microtiter well. Error bars represent the SEM. Data represents 3 independent experiments, each with 6 technical replicates (n=18 per treatment, Welch's t-test).

336

337 **The *lov* mutant is impaired in host attachment, colonization, and virulence.**

338 *In planta* transcriptomics suggested *Rps* attachment, motility, and EPS production were altered in
339 Δ*lov* during tomato infection. *Rps* LOV contains two domains predicted to modulate c-di-GMP, a
340 cosmopolitan secondary messenger that often dictates sessile-motile lifestyle switches in bacteria (29).
341 While wild-type and Δ*lov* did not differ in static biofilm formation or motility *in vitro* (Figure 5A-B),
342 *Rps* did require LOV for normal expression of attachment-related genes *in planta*. Adhesion to the
343 rhizoplane is the first physical interaction in bacterial wilt disease (56). We found that Δ*lov* attached to
344 tomato seedling roots ~70% less frequently than wild-type *Rps* (Figure 5C). The Δ*lov* mutant also had a
345 significant defect in tomato stem colonization after direct inoculation via a cut petiole (Figure 5D). Co-
346 inoculating both strains into a single plant rescued the Δ*lov* colonization defect (Figure S5A).

347 We were intrigued by the conflicting results of our *in vitro* and *in planta* attachment data. The *in*
348 *vitro* transcriptomic and phenotypic experiments suggested LOV is not required for attachment, but the
349 *in planta* gene expression patterns and functional assays suggested otherwise. We tested whether LOV
350 responds to host-derived signals to form biofilms in plant stems by incorporating *ex vivo* tomato xylem
351 sap into an *in vitro* biofilm assay. In the presence of xylem sap, Δ*lov* formed significantly less biofilm
352 than wild-type (Figure 5E). These results suggest LOV contributes to both early (root phase) and late
353 (stem phase) colonization of the host and requires specific plant-derived signals.

354 The Δ*lo*v mutant's altered stress tolerance, nutrient use, and host attachment and colonization
355 behaviors suggested that LOV is required for full virulence. We tested this hypothesis using two
356 different virulence assays. Following a naturalistic soil soak inoculation of unwounded tomato plants,
357 symptoms appeared more slowly on Δ*lov*-inoculated plants but by the end of the assay they reached
358 similar disease index levels as plants inoculated with the wild-type strain (Figure 5F). When the root
359 infection stage was bypassed by inoculating bacteria directly through a cut petiole, Δ*lov* caused delayed
360 wilting and reached a lower final disease index than wild-type (Figure S5B). Since LOV mediated
361 bacterial growth at elevated temperatures *in vitro* (Figure 3A), we wondered if higher temperatures
362 would exacerbate Δ*lov*'s host colonization and virulence defect. Although warmer temperatures did
363 cause higher levels of stem colonization and a faster onset of disease for both genotypes, the magnitude
364 of the Δ*lov* mutant's colonization and virulence defect remained constant across temperatures (Figures
365 S5C-D). Taken together, these experiments demonstrate that LOV is required for full *Rps* virulence.

366

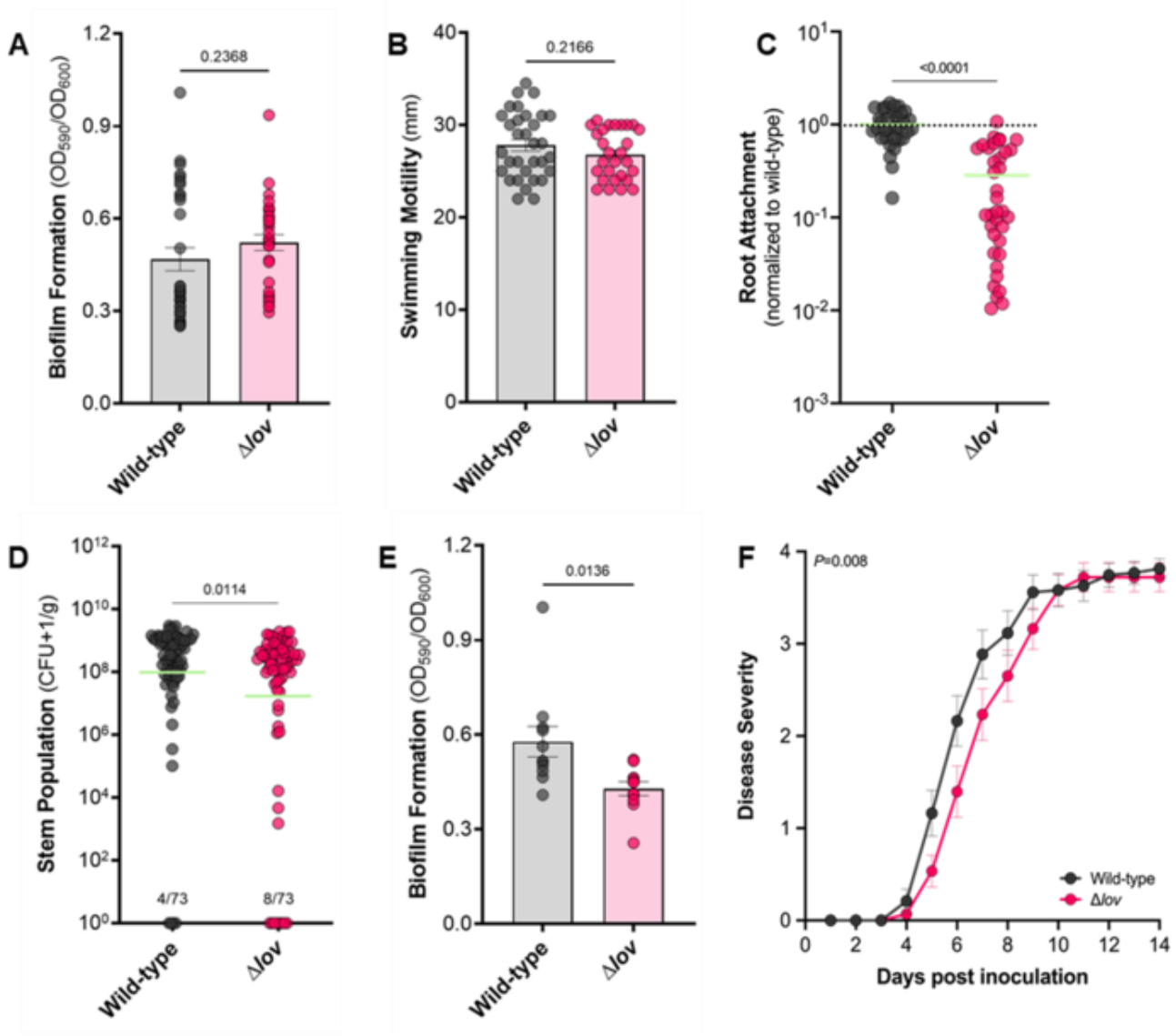

Figure 5: Loss of LOV does not affect *Rps* biofilm or motility *in vitro* but decreases plant-associated fitness traits including root attachment, stem colonization, biofilm formation in xylem sap, and virulence. A) Biofilm formation in rich media. Each circle represents a single microtiter well. Error bars represent the SEM. Data represents 3 independent experiments with 8-12 technical replicates each (n=32 per treatment, Student's t-test). **B)** Motility in rich media. Each circle represents the average of two orthogonal measurements of the diameter of a single colony. Error bars represent the SEM. Data represents 3 independent experiments with 4-12 technical replicates each (n=28-32 per treatment, Welch's t-test). **C)** Attachment to seedling roots. Each symbol represents 4-5 pooled roots, normalized to root biomass. Values were further normalized to wild-type levels; the black dashed line indicates value '1' (mean wild-type attachment). Solid green lines indicate the mean attached population size for each strain. Data represent 4 independent experiments, each with 6-10 technical replicates (n=33-36 per treatment, Welch's t-test). A single outlier identified by a ROUT analysis (default parameters, implemented in GraphPad Prism) was removed prior to analysis and visualization. **D)** Stem colonization. Each circle represents the population in a single plant. Data represents 4 independent experiments with 15-23 plants each (n=73 per treatment, Welch's t-test). Green lines indicate the geometric mean. The number of plants with undetectable *Rps* populations is indicated above the x-axis (limit of detection = ~1000 CFU/g). A value of 1 was added to all final numbers to enable graphing '0' values on a log scale. **E)** Biofilm formation in

385 *ex vivo* xylem sap. Each circle represents a single tube. Bars represent the SEM. Data reflects 4
386 independent experiments with 2-3 technical replicates each (n=11 per treatment, Welch's t-test). **F)** Wilt
387 disease progression following soil soak-inoculation. Data reflects 3 independent experiments, each with
388 13-15 plants (n=43 plants per treatment, RM two-way ANOVA). Error bars represent SEM.
389

390 **Discussion**

391 The striking conservation of LOV across distantly related strains occupying diverse niches
392 suggests this protein with multiple signaling domains is important in *Ralstonia* biology. The N-terminal
393 Cache domain was the least conserved part of the LOV protein. Variation in this extracellular ligand-
394 binding domain may allow diverging *Ralstonia* strains to incorporate unique external cues into the LOV
395 signaling network (57). Further, the well-characterized photoreactive cysteine residue has shifted to a
396 non-reactive alanine in multiple non-pathogenic *Ralstonia* species. A similar Cys-Ala shift between
397 pathogenic and non-pathogenic microorganisms is present in the Sordariomycetes, where homologs of
398 the ENV1 photoreceptor also lack the critical cysteine in non-plant pathogens (22, 58). The absence of
399 this photoreactive cysteine may decouple specific sensory cues, enabling the protein to serve a divergent
400 function (59). This natural sequence diversity could be leveraged to see if the residue shift and Cache
401 domain variations reflect distinct LOV functions in some *Ralstonia* lineages.

402 While LOV has mostly been studied as a blue light photosensor, we demonstrate it has light-
403 independent functions in *Rps*, a soil-borne plant pathogen. RNA-seq has defined the downstream effects
404 of light on several microbes with photoreceptors (27, 60, 61). However, our *in vitro* RNA-seq
405 experiment revealed that blue light has a surprisingly small effect on *Rps* transcription, regardless of the
406 presence of *lov*. The FMN-binding cysteine in the LOV domain can also be activated by redox changes
407 (23), and we hypothesize *Rps* LOV responds to forms of oxidative stress present in the plant
408 environment. A universal stress protein (USP, *rsp1561*) was one of the very few genes that were
409 differentially expressed in Δ*lov* both *in vitro* and *in planta,* albeit in different directions. USPs are multi-
410 functional and respond to a medley of abiotic stressors in prokaryotes and eukaryotes (43, 62, 63). While
411 *Rps* USPs have not been characterized, LOV-mediated changes in USP expression may improve
412 pathogen survival under stressful conditions.

413 LOV proteins regulate the general stress response (GSR) of other Proteobacteria (61, 64–66).
414 While light activates a stress response via LOV in some microbes (25, 26, 67), other studies found GSR
415 is transcriptionally controlled by LOV in the dark (61). In addition to USP *rsp1561*, Δ*lov* also
416 upregulated *rpoS in planta*. This alternative sigma factor is a core regulator of GSR in *E. coli* (68). GSR
417 can be activated by several stressors that we studied (e.g., heat shock, oxidative stress, nutrient changes),
418 and the downstream stress response pathways and physiological changes include phenotypes that were
419 altered in our Δ*lov* mutant (e.g., nutrient scavenging, biofilm formation, and virulence) (69). It has been
420 suggested that inappropriate expression of GSR regulators may alter bacterial resistance to seemingly
421 unrelated stressors – as we observed for Δ*lov* (69). Explicitly investigating the role of *Rps* LOV in GSR
422 regulation would likely be fruitful.

423 In culture, Δ*lov* had increased tolerance to ROS stress, growth in iron-replete conditions, and
424 siderophore production compared to wild-type. Siderophores sequester environmental iron and often
425 improve microbial fitness under iron-limiting conditions (70). However, Δ*lov* had no growth advantage
426 in low-iron media. Rather than improving growth by facilitating iron uptake, siderophore overproduction
427 by Δ*lov* may reduce oxidative stress by sequestering excess iron and preventing toxic Fenton chemistry
428 (54). Cells tightly regulate iron uptake via ferric uptake regulator Fur and the Feo system, in
429 coordination with oxidative stress responses (71–73). Expression of *ahpC*, a critical enzyme for
430 detoxifying peroxides, is regulated by Fur in some microbes (74, 75). The *fur2*, *feoAB*, and *ahpC* genes
431 immediately surround *lov* on the *Rps* GMI1000 megaplasmid. Our redox assay results also support a

432 model of siderophore-mediated protection from oxidative stress. Exogenous H_2O_2 can exacerbate iron
433 toxicity at lower levels, and increased production of siderophore-like molecules may therefore manifest
434 as improved tolerance to oxidative stress (76). The dysregulation of iron- and redox-related phenotypes
435 in the mutant indicates that LOV normally helps balance these cellular responses, but the exact
436 mechanism warrants further investigation.

437 Although adding a wild-type copy of *lov* to the Δ*lov* mutant at the chromosomal *att* locus
438 partially restored wild-type levels of heat tolerance and trended towards wild-type levels of caffeate
439 tolerance, we were not able to complement other phenotypes of Δ*lov*. Regulatory mutants are
440 notoriously difficult to complement in plant pathogenic *Ralstonia* (9), particularly for *in planta*
441 phenotypes. Moreover, proper function of LOV may depend on its highly conserved genomic context.
442 The *lov* gene is flanked by the *aer* redox sensor and a GGDEF-encoding gene of unknown function,
443 which both have regulatory inputs and outputs that could overlap with LOV (29, 77). We cannot rule out
444 post-transcriptional or allosteric effects of protein-protein interactions that depend on appropriate
445 subcellular localization of LOV (78). Further, it is becoming increasingly evident that spatially localized
446 concentrations of c-di-GMP can contribute to cellular phenotypes (79). If LOV affects a local pool of
447 this secondary messenger, this would not be restored by complementation at a remote genomic site.

448 Intracellular c-di-GMP levels often modulate bacterial motility and biofilm formation and
449 *Ralstonia* LOV contains two putative c-di-GMP active domains (29). Our *in vitro* assays and
450 transcriptomics detected no LOV-dependent effect on motility, biofilm, or associated gene expression,
451 but *in planta* experiments painted a very different picture. The Δ*lov* mutant was defective in root
452 attachment and stem colonization, and genes important for RSSC root attachment (*radA*, *pilE*, *rsp1090-*
453 *rsp1092*, and *fliC*) were upregulated in Δ*lov in planta (15, 80, 81)*. The strong root attachment
454 suppressor *lecX* was also upregulated, which could explain the observed adhesion defects (21). Further,
455 using *ex vivo* xylem sap rather than rich media in the *in vitro* biofilm assay revealed a LOV-dependent
456 defect, suggesting LOV affects biofilm formation in response to a plant-derived signal.

457 Extracellular polysaccharides (EPS) generally contribute to biofilm formation (82). Although the
458 EPS I biosynthetic cluster was upregulated in Δ*lov in planta*, the mutant formed normal biofilms *in vitro*
459 in the dark. Because EPS I specifically helps *Rps* form biofilms under flow, the static PVC plate assay
460 cannot capture EPS I-mediated differences in Δ*lov* biofilms (21). Additionally, because EPS can protect
461 bacteria from redox stress, enhanced EPS gene expression by Δ*lov in planta* could indicate the mutant
462 suffers impaired stress resistance. Quantifying Δ*lov* biofilms in tomato stems or in a xylem-mimicking
463 microfluidic system could determine if LOV influences biofilm development in more biologically
464 relevant physical conditions (83). Additionally, targeted mutations in the GGDEF-EAL domains of LOV
465 combined with measurements of cellular c-di-GMP levels are needed to determine the effects of LOV
466 diguanylate cyclase or phosphodiesterase activity under different conditions.

467 A previous study of *Rps lov* in dark and white light conditions reported LOV is essential for any
468 swimming motility, twitching motility, EPS production, biofilm formation, and stem colonization
469 regardless of light treatment (39). We were unable to replicate these findings (Figure S6A). Because the
470 phenotype of the previous mutant resembles that of a Δ*phcA* quorum sensing mutant, we speculate that it
471 resulted from a spontaneous and commonly reported secondary mutation (84). We did probe the specific
472 effect of blue light on several aspects of *Rps* biology and found that blue light enhances *in vitro* biofilm
473 production, represses *in vitro* motility, and represses root attachment in wild-type cells (Figure S6B-D).
474 This effect could be an indirect effect of redox stress induced by the high-energy short wavelength light.
475 Further, the blue light-induced biofilm and root attachment phenotypes were at least partially mediated
476 by LOV (Figures S6B and S6E). However, of the three recent works that investigate the role of *Rps*
477 GMI1000 LOV ((30, 39), this study), none of the reported biofilm and motility phenotypes are
478 consistent. We suspect this discordance is due to the complexity of the LOV signaling network and the
479 currently unknown signal(s) to which it responds. While many of our long-term stress assays with LOV-

480 dependent phenotypes were performed in the dark, our *in planta* colonization and virulence assays
481 required growth chambers with diurnal light cycles. Although we identified several phenotypes
482 controlled by LOV in a light-independent manner, future work employing different light exposure
483 methods will further define light-dependent and -independent roles for LOV in *Rps* biology (27, 85).

484 In addition to the specific LOV domain, the large *Rps* LOV protein contains three other signal
485 input domains that can incorporate multiplexed cues. Together, our transcriptomic and functional data
486 suggest that LOV regulation is highly context-dependent and cannot be captured by reductionist *in vitro*
487 assays. More broadly, host-associated microbes often behave abnormally outside their natural context
488 (31), and mutating other *Rps* regulators has contradictory fitness impacts *in planta* and *in vitro* (9, 11).
489 In the case of Δ*lov*, contrasting fitness outcomes may be due to the mutant altering its GSR to
490 compensate for a loss of LOV-dependent regulation. The regulatory influence of *lov* adds another player
491 to the RSSC regulators critical for life *in planta*, including the virulence and metabolic regulators *phcA*
492 and *efpR*, and the plant-induced type III secretion system *prh* and *hrp* regulons (8, 9, 11, 86–94).

493 We propose that *Rps* LOV regulates multiple functions required for fitness during plant
494 colonization and pathogenesis. Deleting *lov* had very little effect on the *Rps* transcriptome when the
495 bacterium grew in culture, but many more genes were dysregulated in the Δ*lov* mutant during tomato
496 infection. Consistent with this, Δ*lov* grew as well as wild-type in culture but suffered quantitative defects
497 in several plant-associated traits like attachment to roots, biofilm formation in xylem sap, stem
498 colonization, and overall bacterial wilt virulence. The broad dysregulation caused by loss of LOV
499 apparently reduces bacterial fitness in the dynamic host environment. For example, LOV likely helps
500 balance opposing attachment behaviors that are critical for systemic dispersal and symptom
501 development (95). Our data also suggests LOV is required for appropriate redox stress response to resist
502 plant defenses (2). Comparative metabolomics of xylem sap from Δ*lov*- and wild-type-infected plants
503 could test the hypothesis that LOV regulates the ability of *Rps* to degrade plant antimicrobial phenolic
504 compounds, which generate toxic ROS stress.

505 Taken together, our results indicate that *Rps* LOV is a signaling node modulating environmental
506 stress tolerance, nutrient homeostasis, and virulence-related behaviors in response to plant-derived
507 stimuli. LOV may help bacterial wilt pathogens transition between life in oligotrophic surface waters,
508 the nutrient-rich rhizosphere, and the flowing plant xylem (8). Ultimately, our work establishes LOV as
509 one of many critical sensors used by *Rps* to adjust its physiology and effectively cause disease in the
510 dynamic host environment.

511

512 **Materials and Methods**

513 **Bacterial strains and mutants.**

514 *Ralstonia pseudosolanacearum* (*Rps*) phyl. I-seq 18 strain GMI1000 and the Δ*lov* mutant were routinely
515 grown at 28°C in rich medium (CPG; 10 g/L peptone, 1 g/L casamino acids, 5 g/L glucose, 1 g/L yeast
516 extract) or Boucher's minimal medium (BMM; 3.4 g/L KH_2PO_4, 0.5 g/L $(NH_4)_2SO_4$, 0.45 µM $FeSO_4$ x
517 $7H_20$, 0.517 mM $MgSO_4$, 10 mM glucose). *Escherichia coli* was grown at 37°C in LB (10 g/L tryptone,
518 5 g/L yeast extract, 10 g/L NaCl) with 25 mg/L kanamycin when appropriate. Unless otherwise
519 indicated, *Rps* cultures were prepared for experiments as follows: Single colonies from a solid CPG
520 plate were inoculated into CPG broth. Overnight cultures were centrifuged at 6-8,000 x g for 5-10
521 minutes to pellet cells. The supernatant was removed, and cells were resuspended in water. This wash
522 step was repeated up to three times before measuring the optical density (OD_{600}). This suspension was
523 then used to inoculate various media to desired OD_{600} values.

524 The plasmids, primers, and bacterial strains used for experiments are listed in Table S7. Plasmids
525 were routinely extracted using a Zyppy Plasmid Miniprep Kit (Zymo). An unmarked in-frame deletion
526 of *Rps* GMI1000 *lov* was made using the *sacB* positive selection vector pUFR80 as described previously
527 (5). Due to primer design constraints, 78 bp at the end of the 3537 bp gene were not deleted. A
528 mutagenesis vector (pUFR80Δ*lov*) was constructed with Gibson assembly and transformed into
529 GMI1000 via electroporation (96). Gibson assembly was also used to construct two complementation
530 vectors for insertion at the neutral *att* site: 1) pRCK-lov_{C672A}, a *lov* ORF with the conserved cysteine
531 substituted with alanine, and 2) pRCK-*lov*, the wild-type *lov* ORF. Both vectors included the native
532 promoter and were transformed into Δ*lov* via natural transformation, producing Δ*lov*+lov_{C672A} and
533 Δ*lov*+*lov* (96). The mutations and complementations were confirmed with PCR amplification and
534 sequencing. For experimental assays using the complemented strains, a wild-type and Δ*lov* strain
535 containing empty pRCK inserts were used to control for the vector itself. Additionally, Δ*lov* was
536 naturally transformed with an empty pRCG vector to create an additional antibiotic-resistant strain for
537 competitive colonization experiments. All pRCK- and pRCG-containing strains were selected for using
538 media + kanamycin or gentamycin (both 25 mg/L) as needed.

539 **Plant maintenance and growth conditions.**

540 Tomato plants (wilt-susceptible cv. 'Bonny Best') were routinely grown at 28°C in a climate
541 chamber with a 12-hour photoperiod. Seeds were sown in trays filled with growing mix (Jolly Gardener
542 PRO-LINE C/GP Germinating Mix, Oldcastle Lawn and Garden), covered with a plastic lid to increase
543 humidity, and kept consistently moist until transplanting to 4-inch pots containing ~80 grams of soil at
544 14 days old. Once transplanted, plants were watered with a rotation of water and fertilizer (1/2-strength
545 Hoagland's solution).

546 **Transcriptomic analyses.**

547 <u>*in vitro* experimental design:</u> Three independent overnight cultures of wild-type GMI1000 and
548 Δ*lov* were grown in CPG to an OD_{600} 0.2-0.6. Cells were washed as described above and resuspended to
549 a final OD_{600} of 0.2 in 8 mL of CPG. Cultures were transferred to a small 60 mm petri dish to maximize
550 even light exposure and dark treatment plates were wrapped in foil. Plates were shaken at 100 rpm under
551 blue light (24-25 lux) for 2 hours. Following incubation, stop solution (5% phenol in ethanol) was added
552 to the cultures and cells were pelleted by centrifugation for 5 min at 10,000 rpm.

553 <u>*in planta* experimental design:</u> Wild-type GMI1000 and Δ*lov* cultures were prepared as described
554 above and resuspended in water to a final OD_{600} of 0.001. Three-week-old plants were petiole inoculated
555 with ~2000 colony forming units (CFUs) of GMI1000 or Δ*lov*. Three days post-inoculation, two ~100

556 mg stem samples were collected from each plant: 1) a section taken above the site of inoculation was
557 flash frozen in liquid nitrogen and stored at -80°C prior to RNA extraction, and 2) a section harvested
558 below the site of inoculation was used to quantify the bacterial population (see "Virulence and stem
559 colonization" methods). Selected samples were ground in stop solution using a PowerLyzer bead beater
560 and pelleted by centrifugation for 5 min at 10,000 rpm.

561 RNA extraction, sequencing, and analysis: Following sample centrifugation, the supernatant was
562 discarded and total RNA was extracted from the pellet using the previously described hot phenol-
563 chloroform extraction method (31). The RNA from each sample was extracted individually, measured
564 for quality, and then 2-4 high quality samples were pooled per biological replicate. The *in vitro*
565 experiment was repeated three times, and the *in planta* experiment was repeated four times. RNA
566 samples were sent to Novogene (Beijing) for library preparation, sequencing, and data analysis, which
567 were performed as described previously (10). Due to incongruent gene expression compared to other
568 replicates, one sample from the *in planta* dataset (wild-type) was removed from the final analysis. The
569 final gene expression datasets (Table S3 and S4) were manually filtered based on significance values (q-
570 value < 0.05; p-value < 0.05) as indicated in the text. All transcriptomic data is available in the Gene
571 Expression Omnibus (GEO) database (Accession Number GSE298975) on NCBI.

572 **Oxidative, heat, iron, osmotic and phenolic compound-induced stress assays.**

573 All chronic environmental stress assays measured bacterial growth (OD_{600}) every 30 min for 45-
574 48 hours with a BioTek plate reader. Strains were prepared as described above and normalized in
575 appropriate media to an OD_{600} of 0.01 (unless otherwise stated). Cell suspensions were aliquoted into
576 flat-bottomed 96-well plates (200 µL/well, Corning Costar Ref# 3370) and incubated with continuous
577 shaking. For oxidative stress assays, strains were grown for 48 hours at 28°C with slow shaking in
578 BMM + 1.25 mM hydrogen peroxide (H_2O_2). For heat stress experiments, strains were grown in CPG
579 with slow shaking for 46 hours at 37°C. For ferric iron growth assays, strains were grown for 46 hours at
580 28°C with fast shaking in BMM + 1x (0.417 µM), 10x (4.17 µM), or 100x (41.7 µM) levels of $FeCl_3$ x
581 $6H_2O$. Ferrous iron growth assays were performed similarly, with slightly modified concentrations of
582 $FeSO_4$ x $7H_2O$ (1x = 0.45 µM, 10x = 4.5 µM, 100x = 45 µM). For osmotic stress assays, strains were
583 grown for 46 hours at 28°C with medium shaking in CPG + 0.15 M NaCl. For phenolic stress assays, we
584 modified a previously reported HCA toxicity assay (4). Briefly, GMI1000 and Δ*lov* were normalized to
585 an OD_{600} of 0.001 in modified BMM (10 mM succinate instead of glucose; buffered to pH 5.5 with 10
586 mM MES) + caffeate (750 µM or 1250µM). The strains were grown at 28°C with slow shaking for 48
587 hours (750 µM) or 72 hours (1250 µM).

588 **Growth in *ex vivo* xylem sap.**

589 Xylem sap was collected from 5-week-old tomato plants as described previously (97, 98), with
590 minor modifications as follows: after de-topping plants, sap was collected for 3 hours and pooled into a
591 single pre-chilled 50 mL tube on ice. Sap was filter-sterilized (0.22 µm), aliquoted into 1 ml volumes,
592 frozen at -20°C, and used for experiments within 3 weeks of collection. For growth curves, cultures
593 were prepared as described above and resuspended to a final OD_{600} of 0.01 in thawed xylem sap. Cell
594 suspensions were aliquoted into flat-bottomed 96-well plates (200 µL/well, Corning Costar Ref# 3370)
595 and incubated at 28°C with slow continuous shaking in a Biotek plate reader. The OD_{600} was measured
596 every 30 minutes for 24 hours.

597 **Growth on various carbon sources.**

598 Strains were prepared as described above and resuspended to a final OD_{600} of 0.07 in BMM
599 without glucose (no exogenous carbon). The suspensions were then aliquoted into Biolog Ecoplates (125
600 µL/well, Biolog, Inc., Hayward, California) and an initial OD_{590} measurement was immediately taken
601 using a BioTek plate reader. The plates were incubated statically at 28°C and the OD_{590} was measured

602 daily for 1 week. For analysis, the initial OD_{590} reading was subtracted from all subsequent readings to
603 control for background interference. The OD_{590} reading for the water control wells was then subtracted
604 from all treatments at each timepoint to adjust for growth in the control. Negative values were adjusted
605 to '0' before analysis. These values were then used to calculate the AUC for each well over the 7 day
606 incubation period.

607 **Siderophore production.**

608 *Rps* GMI1000 wild-type and *Δlov* strains were prepared as described above and resuspended to a
609 final OD_{600} of 0.01 in modified BMM (0.85 g/L KH_2PO_4, 0.5 g/L $(NH_4)_2SO_4$, 0.417 µM $FeCl_3$ x $6H_2O$,
610 0.517 mM $MgSO_4$, 10 mM glucose, buffered to pH 7 with 10 mM MES). Resuspended cultures were
611 aliquoted into round-bottom 96-well plates (200 µL/well, Dot Scientific Product #229590). The lids
612 were secured with parafilm and incubated with continuous shaking (180 rpm) at 28°C. After 24 hours,
613 wells were mixed by pipetting to resuspend settled cells and the OD_{600} was measured using a Biotek
614 plate reader. Plates were centrifuged for 20 minutes at 3,500 rpm to pellet cells. One hundred microliters
615 of the supernatant was transferred to a fresh 96-well plate and mixed 1:1 with CAS reagent (99, 100).
616 Control samples were prepared by mixing sterile BMM medium with CAS. The OD_{630} of the
617 supernatant:CAS mixtures were measured on a Biotek plate reader. Final values were calculated using
618 the following equation: $((A_c-A_s)*100)/A_c$; where A_c = absorbance of the control, A_s = absorbance of
619 supernatant sample. Values were then divided by the OD_{600} of the corresponding well to account for
620 growth differences.

621 **Biofilm formation.**

622 Strains were prepared as described above. Static biofilm assays in rich media were performed as
623 described (21), with slight modifications as follows: biofilms were stained with 150 µL 0.1% crystal
624 violet for 20 minutes, washed three times with 200 µL sterile water, and de-stained with 200 µL of 95%
625 ethanol for 20 minutes.

626 For assays done in *ex vivo* xylem sap, strains were resuspended to an OD_{600} 0.01 in sap.
627 Suspensions were aliquoted (1.4 mL per tube) into small borosilicate glass tubes. The top of each tube
628 was wrapped in parafilm and a loose-fitting cap was placed on top. Tubes were incubated statically at
629 28°C for 5 days. After the incubation period, the suspension was gently mixed using a pipette and the
630 OD_{600} was measured. The cellular suspension was removed and the tube was gently washed with 2 mL
631 of water. The biofilms were stained with 2 mL 0.1% crystal violet for 20 minutes, washed once with 2
632 mL water, and de-stained with 2 mL of 95% ethanol for 20 minutes with shaking. The resulting solution
633 was measured at OD_{590} and normalized by the initial OD_{600}.

634 **Swimming motility.**

635 Strains were prepared as described above and resuspended at OD_{600} 0.1 in water. Four 2 µL
636 droplets of *Rps* GMI1000 or Δ*lov* were equidistantly placed on 100 mm square petri plates filled with
637 semi-solid motility media (BMM + 1% tryptone + 0.3% Bacto Agar (BD Difco)). Plates were sealed
638 with Micropore tape and incubated at 28°C for 40 hours. Two orthogonal measurements of each colony
639 diameter were taken and averaged.

640 **Root attachment.**

641 Rhizoplane populations were measured as described (15, 97) with minor modifications as
642 follows: seedlings were flood-inoculated with 15 mL of 10^6 CFU/mL (OD_{600} 0.001) *Rps* GMI1000 or
643 Δ*lov* suspended in water. The cellular suspension was removed after 2 hours and the seedlings were
644 flooded with sterile water, swirled for 10 seconds, and water was removed. Seedlings were cut to
645 separate the root from the hypocotyl, blotted dry, and pooled together (4-5 roots per technical replicate).
646 Each pooled sample of roots was weighed before homogenization.

647 **Virulence and stem colonization.**

648 Plant assays were performed as described (97). Briefly, 21-day-old plants were either soil soak-
649 inoculated or petiole-inoculated with GM1000 or Δ*lov* cells to assess virulence. Symptom development
650 was rated for 14 days. For stem colonization, plants were petiole-inoculated with GM1000 or Δ*lov*.
651 Three days post-infection, approximately 100 mg of stem directly below the cut petiole was
652 homogenized in water. Samples were diluted and plated to quantify CFU/gram.

653 **Statistical Analysis**

654 All statistics and area under the curve (AUC) calculations were performed using GraphPad Prism
655 version 10, GraphPad Software, San Diego, California USA, https://www.graphpad.com/. Specific
656 statistical tests used for analysis are indicated in each figure legend and P-values are reported in the
657 graph or figure legend where necessary.

658

659 **Acknowledgments**

660 We gratefully acknowledge Shabda Gajbhiye and Mairead Morahan for their technical
661 assistance.

662

663 **Supplemental Figures and Tables**

664 **Figure S1:** The *lov* gene is conserved across *Ralstonia*, along with a 12-gene syntenic cluster.

665 **Figure S2:** LOV differentially influences bacterial growth and survival under diverse stressors.

666 **Figure S3:** *Rps* wild-type has a slight growth advantage over the Δ*lov* mutant in many, but not all,
667 carbon sources.

668 **Figure S4:** Deleting *lov* reduces *Rps* growth on selected carbon sources under acidic conditions.

669 **Figure S5:** *Rps* GMI1000 Δ*lov* has a host colonization and virulence defect at both 28°C and 32°C.

670 **Figure S6.** Blue light modestly influences *Rps* behavior in both LOV-dependent and LOV-independent
671 ways.

672

673 **Table S1:** List of 111 *Ralstonia spp.* genomes included in *lov* bioinformatic analyses.

674 **Table S2:** LOV genomic region in *Ralstonia*.

675 **Table S3:** Results from *in vitro* RNA-seq.

676 **Table S4:** Results from *in planta* RNA-seq.

677 **Table S5:** Growth in Biolog Ecoplates (Area Under Curve).

678 **Table S6:** Growth in PM10 Biolog Plates (Area Under Curve).

679 **Table S7:** Bacterial strains, plasmids, and primers used in this study.

680

681 **References**

682 1. Compant S, Cambon MC, Vacher C, Mitter B, Samad A, Sessitsch A. 2021. The plant endosphere
683 world - bacterial life within plants. Environ Microbiol 23:1812–1829.

684 2. Flores-Cruz Z, Allen C. 2009. *Ralstonia solanacearum* encounters an oxidative environment during
685 tomato infection. Mol Plant Microbe Interact 22:773–782.

686 3. Flores-Cruz Z, Allen C. 2011. Necessity of OxyR for the hydrogen peroxide stress response and full
687 virulence in *Ralstonia solanacearum*. Appl Environ Microbiol 77:6426–6432.

688 4. Lowe TM, Ailloud F, Allen C. 2015. Hydroxycinnamic Acid Degradation, a Broadly Conserved
689 Trait, Protects *Ralstonia solanacearum* from Chemical Plant Defenses and Contributes to Root
690 Colonization and Virulence. Mol Plant Microbe Interact 28:286–297.

691 5. Lowe-Power TM, Jacobs JM, Ailloud F, Fochs B, Prior P, Allen C. 2016. Degradation of the Plant
692 Defense Signal Salicylic Acid Protects *Ralstonia solanacearum* from Toxicity and Enhances
693 Virulence on Tobacco. MBio 7.

694 6. Hamilton CD, Zaricor B, Dye CJ, Dresserl E, Michaels R, Allen C. 2023. *Ralstonia solanacearum*
695 pandemic lineage strain UW551 overcomes inhibitory xylem chemistry to break tomato bacterial
696 wilt resistance. Mol Plant Pathol https://doi.org/10.1111/mpp.13395.

697 7. Zhang Y, Zhang W, Han L, Li J, Shi X, Hikichi Y, Ohnishi K. 2019. Involvement of a PadR
698 regulator PrhP on virulence of *Ralstonia solanacearum* by controlling detoxification of phenolic
699 acids and type III secretion system. Mol Plant Pathol 20:1477–1490.

700 8. Vailleau F, Genin S. 2023. *Ralstonia solanacearum*: An Arsenal of Virulence Strategies and
701 Prospects for Resistance. Annu Rev Phytopathol 61:25–47.

702 9. Khokhani D, Lowe-Power TM, Tran TM, Allen C. 2017. A Single Regulator Mediates Strategic
703 Switching between Attachment/Spread and Growth/Virulence in the Plant Pathogen *Ralstonia*
704 *solanacearum*. MBio 8.

705 10. Hendrich CG, Truchon AN, Dalsing BL, Allen C. 2023. Nitric oxide regulates the *Ralstonia*
706 *solanacearum* type III secretion system. Mol Plant Microbe Interact 36:334–344.

707 11. Perrier A, Peyraud R, Rengel D, Barlet X, Lucasson E, Gouzy J, Peeters N, Genin S, Guidot A.
708 2016. Enhanced *in planta* fitness through adaptive mutations in EfpR, a dual regulator of virulence
709 and metabolic functions in the plant pathogen *Ralstonia solanacearum*. PLoS Pathog 12:e1006044.

710 12. Tsuzuki M, Inoue K, Kiba A, Ohnishi K, Kai K, Hikichi Y. 2023. Infection route in tomato roots
711 and quorum sensing of *Ralstonia pseudosolanacearum* strain OE1-1. Physiol Mol Plant Pathol
712 125:101995.

713 13. Yao J, Allen C. 2007. The plant pathogen *Ralstonia solanacearum* needs aerotaxis for normal
714 biofilm formation and interactions with its tomato host. J Bacteriol 189:6415–6424.

715 14. Yao J, Allen C. 2006. Chemotaxis is required for virulence and competitive fitness of the bacterial
716 wilt pathogen *Ralstonia solanacearum*. J Bacteriol 188:3697–3708.

717 15. Carter MD, Khokhani D, Allen C. 2023. Cell Density-Regulated Adhesins Contribute to Early
718 Disease Development and Adhesion in *Ralstonia solanacearum*. Appl Environ Microbiol
719 89:e0156522.

720 16. Rivera-Zuluaga K, Hiles R, Barua P, Caldwell D, Iyer-Pascuzzi AS. 2023. Getting to the root of
721 *Ralstonia* invasion. Semin Cell Dev Biol 148-149:3–12.

722 17. Lowe-Power TM, Khokhani D, Allen C. 2018. How *Ralstonia solanacearum* Exploits and Thrives
723 in the Flowing Plant Xylem Environment. Trends Microbiol 26:929–942.

724 18. Dalsing BL, Truchon AN, Gonzalez-Orta ET, Milling AS, Allen C. 2015. *Ralstonia solanacearum*
725 uses inorganic nitrogen metabolism for virulence, ATP production, and detoxification in the
726 oxygen-limited host xylem environment. MBio 6:e02471.

727 19. Truchon AN, Dalsing BL, Khokhani D, MacIntyre A, McDonald BR, Ailloud F, Klassen J,
728 Gonzalez-Orta ET, Currie C, Prior P, Lowe-Power TM, Allen C. 2023. Plant-Pathogenic *Ralstonia*
729 Phylotypes Evolved Divergent Respiratory Strategies and Behaviors To Thrive in Xylem. MBio
730 14:e0318822.

731 20. Ingel B, Caldwell D, Duong F, Parkinson DY, McCulloh KA, Iyer-Pascuzzi AS, McElrone AJ,
732 Lowe-Power TM. 2022. Revisiting the source of wilt symptoms: X-ray microcomputed tomography
733 provides direct evidence that *Ralstonia* biomass clogs xylem vessels. PhytoFront 2:41–51.

734 21. Carter MD, Tran TM, Cope-Arguello ML, Weinstein S, Li H, Hendrich CG, Prom JL, Li J, Chu LT,
735 Bui L, Manikantan H, Lowe-Power TM, Allen C. 2024. Lectins and polysaccharide EPS I have
736 flow-responsive roles in the attachment and biofilm mechanics of plant pathogenic *Ralstonia*. PLoS
737 Pathog 20:e1012358.

738 22. Beattie GA, Hatfield BM, Dong H, McGrane RS. 2018. Seeing the Light: The Roles of Red- and
739 Blue-Light Sensing in Plant Microbes. Annu Rev Phytopathol 56:41–66.

740 23. Losi A, Gärtner W. 2017. Solving blue light riddles: New lessons from flavin-binding LOV
741 photoreceptors. Photochem Photobiol 93:141–158.

742 24. Losi A, Gärtner W. 2021. A light life together: photosensing in the plant microbiota. Photochem
743 Photobiol Sci 20:451–473.

744 25. Ondrusch N, Kreft J. 2011. Blue and red light modulates SigB-dependent gene transcription,
745 swimming motility and invasiveness in *Listeria monocytogenes*. PLoS One 6:e16151.

746 26. Moriconi V, Sellaro R, Ayub N, Soto G, Rugnone M, Shah R, Pathak GP, Gärtner W, Casal JJ.
747 2013. LOV-domain photoreceptor, encoded in a genomic island, attenuates the virulence of
748 *Pseudomonas syringae* in light-exposed Arabidopsis leaves. Plant J 76:322–331.

749 27. Hatfield BM, LaSarre B, Liu M, Dong H, Nettleton D, Beattie GA. 2023. Light cues induce
750 protective anticipation of environmental water loss in terrestrial bacteria. Proc Natl Acad Sci U S A
751 120:e2309632120.

752 28. Bonomi HR, Posadas DM, Paris G, Carrica M del C, Frederickson M, Pietrasanta LI, Bogomolni
753 RA, Zorreguieta A, Goldbaum FA. 2012. Light regulates attachment, exopolysaccharide
754 production, and nodulation in *Rhizobium leguminosarum* through a LOV-histidine kinase
755 photoreceptor. Proc Natl Acad Sci U S A 109:12135–12140.

756 29. Hengge R. 2009. Principles of c-di-GMP signalling in bacteria. Nat Rev Microbiol 7:263–273.

757 30. Li X, Yin W, Lin JD, Zhang Y, Guo Q, Wang G, Chen X, Cui B, Wang M, Chen M, Li P, He Y-W,
758 Qian W, Luo H, Zhang L-H, Liu X-W, Song S, Deng Y. 2023. Regulation of the physiology and
759 virulence of *Ralstonia solanacearum* by the second messenger 2’,3'-cyclic guanosine
760 monophosphate. Nat Commun 14:7654.

761 31. Jacobs JM, Babujee L, Meng F, Milling A, Allen C. 2012. The *in planta* transcriptome of *Ralstonia*
762 *solanacearum*: conserved physiological and virulence strategies during bacterial wilt of tomato.
763 MBio 3.

764 32. Schuhmacher L, Heck S, Pitz M, Mathey E, Lamparter T, Blumhofer A, Leister K, Fischer R. 2024.
765 The LOV-domain blue-light receptor LreA of the fungus *Alternaria alternata* binds predominantly
766 FAD as chromophore and acts as a light and temperature sensor. J Biol Chem 300:107238.

767 33. Herrou J, Crosson S. 2011. Function, structure and mechanism of bacterial photosensory LOV
768 proteins. Nat Rev Microbiol 9:713–723.

769 34. Purcell EB, McDonald CA, Palfey BA, Crosson S. 2010. An analysis of the solution structure and
770 signaling mechanism of LovK, a sensor histidine kinase integrating light and redox signals.
771 Biochemistry 49:6761–6770.

772 35. Milling A, Babujee L, Allen C. 2011. *Ralstonia solanacearum* extracellular polysaccharide is a
773 specific elicitor of defense responses in wilt-resistant tomato plants. PLoS One 6:e15853.

774 36. Truchon AN, Hendrich CG, Bigott AF, Dalsing BL, Allen C. 2022. NorA, HmpX, and NorB
775 Cooperate to Reduce NO Toxicity during Denitrification and Plant Pathogenesis in *Ralstonia*
776 *solanacearum*. Microbiol Spectr 10:e0026422.

777 37. Krauss U, Minh BQ, Losi A, Gärtner W, Eggert T, von Haeseler A, Jaeger K-E. 2009. Distribution
778 and phylogeny of light-oxygen-voltage-blue-light-signaling proteins in the three kingdoms of life. J
779 Bacteriol 191:7234–7242.

780 38. Losi A, Mandalari C, Gärtner W. 2014. From plant infectivity to growth patterns: The role of Blue-
781 Light sensing in the prokaryotic world. Plants 3:70–94.

782 39. Tano J, Ripa MB, Tondo ML, Carrau A, Petrocelli S, Rodriguez MV, Ferreira V, Siri MI, Piskulic
783 L, Orellano EG. 2021. Light modulates important physiological features of *Ralstonia*
784 *pseudosolanacearum* during the colonization of tomato plants. Sci Rep 11:14531.

785 40. Henry JT, Crosson S. 2011. Ligand-binding PAS domains in a genomic, cellular, and structural
786 context. Annu Rev Microbiol 65:261–286.

787 41. Xing J, Gumerov VM, Zhulin IB. 2023. Origin and functional diversification of PAS domain, a
788 ubiquitous intracellular sensor. Sci Adv 9:eadi4517.

789 42. Glantz ST, Carpenter EJ, Melkonian M, Gardner KH, Boyden ES, Wong GK-S, Chow BY. 2016.
790 Functional and topological diversity of LOV domain photoreceptors. Proc Natl Acad Sci U S A
791 113:E1442–51.

792 43. Kvint K, Nachin L, Diez A, Nyström T. 2003. The bacterial universal stress protein: function and
793 regulation. Curr Opin Microbiol 6:140–145.

794 44. Gustavsson N, Diez A, Nyström T. 2002. The universal stress protein paralogues of *Escherichia*
795 *coli* are co-ordinately regulated and co-operate in the defence against DNA damage. Mol Microbiol
796 43:107–117.

797 45. Elphinstone JG. 2005. The current bacterial wilt situation: a global overview. American
798 Phytopathological Society (APS Press), St. Paul, MN, USA.

799 46. Yu X, Feng B, He P, Shan L. 2017. From Chaos to Harmony: Responses and Signaling upon
800 Microbial Pattern Recognition. Annu Rev Phytopathol 55:109–137.

801 47. Naoumkina MA, Zhao Q, Gallego-Giraldo L, Dai X, Zhao PX, Dixon RA. 2010. Genome-wide
802 analysis of phenylpropanoid defence pathways: Phenylpropanoid defence pathways. Mol Plant
803 Pathol 11:829–846.

804 48. Vanitha SC, Niranjana SR, Umesha S. 2009. Role of phenylalanine ammonia lyase and polyphenol
805 oxidase in host resistance to bacterial wilt of tomato. J Phytopathol (1986) 157:552–557.

806 49. Ishihara T, Mitsuhara I, Takahashi H, Nakaho K. 2012. Transcriptome analysis of quantitative
807 resistance-specific response upon *Ralstonia solanacearum* infection in tomato. PLoS One 7:e46763.

808 50. Hamilton CD, Steidl OR, MacIntyre AM, Hendrich CG, Allen C. 2021. *Ralstonia solanacearum*
809 Depends on Catabolism of Myo-Inositol, Sucrose, and Trehalose for Virulence in an Infection
810 Stage-Dependent Manner. Mol Plant Microbe Interact 34:669–679.

811 51. Gerlin L, Escourrou A, Cassan C, Maviane Macia F, Peeters N, Genin S, Baroukh C. 2021.
812 Unravelling physiological signatures of tomato bacterial wilt and xylem metabolites exploited by
813 *Ralstonia solanacearum*. Environ Microbiol 23:5962–5978.

814 52. Baroukh C, Zemouri M, Genin S. 2022. Trophic preferences of the pathogen *Ralstonia*
815 *solanacearum* and consequences on its growth in xylem sap. Microbiologyopen 11:e1240.

816 53. Murdoch CC, Skaar EP. 2022. Nutritional immunity: the battle for nutrient metals at the host-
817 pathogen interface. Nat Rev Microbiol 20:657–670.

818 54. Arnold E. 2024. Non-classical roles of bacterial siderophores in pathogenesis. Front Cell Infect
819 Microbiol 14:1465719.

820 55. Lau CKY, Krewulak KD, Vogel HJ. 2016. Bacterial ferrous iron transport: the Feo system. FEMS
821 Microbiol Rev 40:273–298.

822 56. Knights HE, Jorrin B, Haskett TL, Poole PS. 2021. Deciphering bacterial mechanisms of root
823 colonization. Environ Microbiol Rep 13:428–444.

824 57. Upadhyay AA, Fleetwood AD, Adebali O, Finn RD, Zhulin IB. 2016. Cache domains that are
825 homologous to, but different from PAS domains comprise the largest superfamily of extracellular
826 sensors in prokaryotes. PLoS Comput Biol 12:e1004862.

827 58. Lokhandwala J, Hopkins HC, Rodriguez-Iglesias A, Dattenböck C, Schmoll M, Zoltowski BD.
828 2015. Structural biochemistry of a fungal LOV domain photoreceptor reveals an evolutionarily
829 conserved pathway integrating light and oxidative stress. Structure 23:116–125.

830 59. Yee EF, Diensthuber RP, Vaidya AT, Borbat PP, Engelhard C, Freed JH, Bittl R, Möglich A, Crane
831 BR. 2015. Signal transduction in light-oxygen-voltage receptors lacking the adduct-forming
832 cysteine residue. Nat Commun 6:10079.

833 60. Santamaría-Hernando S, Rodríguez-Herva JJ, Martínez-García PM, Río-Álvarez I, González-
834 Melendi P, Zamorano J, Tapia C, Rodríguez-Palenzuela P, López-Solanilla E. 2018. *Pseudomonas*
835 *syringae* pv. tomato exploits light signals to optimize virulence and colonization of leaves. Environ
836 Microbiol 20:4261–4280.

837 61. Fiebig A, Varesio LM, Alejandro Navarreto X, Crosson S. 2019. Regulation of the *Erythrobacter*
838 *litoralis* DSM 8509 general stress response by visible light. Mol Microbiol 112:442–460.

839 62. Nachin L, Nannmark U, Nyström T. 2005. Differential roles of the universal stress proteins of
840 *Escherichia coli* in oxidative stress resistance, adhesion, and motility. J Bacteriol 187:6265–6272.

841 63. Luo D, Wu Z, Bai Q, Zhang Y, Huang M, Huang Y, Li X. 2023. Universal stress proteins: From
842 gene to function. Int J Mol Sci 24:4725.

843 64. Kim H-S, Willett JW, Jain-Gupta N, Fiebig A, Crosson S. 2014. The *Brucella abortus* virulence
844 regulator, LovhK, is a sensor kinase in the general stress response signalling pathway. Mol
845 Microbiol 94:913–925.

846 65. Foreman R, Fiebig A, Crosson S. 2012. The LovK-LovR two-component system is a regulator of
847 the general stress pathway in *Caulobacter crescentus*. J Bacteriol 194:3038–3049.

848 66. Sycz G, Carrica MC, Tseng T-S, Bogomolni RA, Briggs WR, Goldbaum FA, Paris G. 2015. LOV
849 Histidine Kinase Modulates the General Stress Response System and Affects the *virB* Operon
850 Expression in *Brucella abortus*. PLoS One 10:e0124058.

851 67. Avila-Pérez M, Hellingwerf KJ, Kort R. 2006. Blue light activates the σ^B-dependent stress response
852 of *Bacillus subtilis* via YtvA. J Bacteriol 188:6411–6414.

853 68. Battesti A, Majdalani N, Gottesman S. 2011. The RpoS-mediated general stress response in
854 *Escherichia coli*. Annu Rev Microbiol 65:189–213.

855 69. Bouillet S, Bauer TS, Gottesman S. 2024. RpoS and the bacterial general stress response. Microbiol
856 Mol Biol Rev 88:e0015122.

857 70. Kramer J, Özkaya Ö, Kümmerli R. 2020. Bacterial siderophores in community and host
858 interactions. Nat Rev Microbiol 18:152–163.

859 71. Pinochet-Barros A, Helmann JD. 2018. Redox sensing by Fe2+ in bacterial Fur family
860 metalloregulators. Antioxid Redox Signal 29:1858–1871.

861 72. Huang M, Wang M, Feng Y, Wang M, Gao Q, Zhu D, Jia R, Chen S, Zhao X, Yang Q, Wu Y,
862 Zhang S, Tian B, Huang J, Ou X, Mao S, Sun D, He Y, Wu Z, Cheng A, Liu M. 2023. Functional
863 characterization of FeoAB in iron acquisition and pathogenicity in *Riemerella anatipestifer*.
864 Microbiol Spectr 11:e0137323.

865 73. Cornelis P, Wei Q, Andrews SC, Vinckx T. 2011. Iron homeostasis and management of oxidative
866 stress response in bacteria. Metallomics 3:540–549.

867 74. Lee H-N, Lee N-O, Han SJ, Ko I-J, Oh J-I. 2014. Regulation of the *ahpC* gene encoding alkyl
868 hydroperoxide reductase in *Mycobacterium smegmatis*. PLoS One 9:e111680.

869 75. Baillon ML, van Vliet AH, Ketley JM, Constantinidou C, Penn CW. 1999. An iron-regulated alkyl
870 hydroperoxide reductase (AhpC) confers aerotolerance and oxidative stress resistance to the
871 microaerophilic pathogen *Campylobacter jejuni*. J Bacteriol 181:4798–4804.

872 76. Galaris D, Barbouti A, Pantopoulos K. 2019. Iron homeostasis and oxidative stress: An intimate
873 relationship. Biochim Biophys Acta Mol Cell Res 1866:118535.

874 77. Maschmann ZA, Chua TK, Chandrasekaran S, Ibáñez H, Crane BR. 2022. Redox properties and
875 PAS domain structure of the *Escherichia coli* energy sensor Aer indicate a multistate sensing
876 mechanism. J Biol Chem 298:102598.

877 78. Valentini M, Filloux A. 2019. Multiple Roles of c-di-GMP Signaling in Bacterial Pathogenesis.
878 Annu Rev Microbiol 73:387–406.

879 79. Hengge R. 2021. High-specificity local and global c-di-GMP signaling. Trends Microbiol 29:993–
880 1003.

881 80. Kang Y, Liu H, Genin S, Schell MA, Denny TP. 2002. *Ralstonia solanacearum* requires type 4 pili
882 to adhere to multiple surfaces and for natural transformation and virulence: *R. solanacearum* type 4
883 pili. Mol Microbiol 46:427–437.

884 81. Corral J, Sebastià P, Coll NS, Barbé J, Aranda J, Valls M. 2020. Twitching and Swimming Motility
885 Play a Role in *Ralstonia solanacearum* Pathogenicity. mSphere 5.

886 82. Limoli DH, Jones CJ, Wozniak DJ. 2015. Bacterial extracellular polysaccharides in biofilm
887 formation and function, p. 223–247. *In* Microbial Biofilms. ASM Press, Washington, DC, USA.

888 83. Chu LT, Laxman D, Abdelhamed J, Pirlo RK, Fan F, Wagner N, Tran TM, Bui L. 2024.
889 Development of a tomato xylem-mimicking microfluidic system to study *Ralstonia*
890 *pseudosolanacearum* biofilm formation. Front Bioeng Biotechnol 12:1395959.

891 84. Kelman A. 1955. The relationship of pathogenicity of *Pseudomonas solanacearum* to colony
892 appearance in a tetrazolium medium. CABI Databases.
893 https://www.cabidigitallibrary.org/doi/full/10.5555/19551101405. Retrieved 27 May 2025.

894 85. Wu L, McGrane RS, Beattie GA. 2013. Light regulation of swarming motility in *Pseudomonas*
895 *syringae* integrates signaling pathways mediated by a bacteriophytochrome and a LOV protein.
896 MBio 4.

897 86. Peyraud R, Cottret L, Marmiesse L, Genin S. 2018. Control of primary metabolism by a virulence
898 regulatory network promotes robustness in a plant pathogen. Nat Commun 9:418.

899 87. Perrier A, Barlet X, Rengel D, Prior P, Poussier S, Genin S, Guidot A. 2019. Spontaneous
900 mutations in a regulatory gene induce phenotypic heterogeneity and adaptation of *Ralstonia*
901 *solanacearum* to changing environments: Phenotypic heterogeneity in *Ralstonia solanacearum*.
902 Environ Microbiol 21:3140–3152.

903 88. Zhang Y, Kiba A, Hikichi Y, Ohnishi K. 2011. prhKLM genes of *Ralstonia solanacearum* encode
904 novel activators of *hrp* regulon and are required for pathogenesis in tomato: New activators of the
905 *hrp* regulon in *R. solanacearum*. FEMS Microbiol Lett 317:75–82.

906 89. Cao Y, Tsuzuki M, Kiba A, Hikichi Y, Zhang Y, Ohnishi K. 2025. Sucrose and malic acid in the
907 tobacco plant induce *hrp* regulon in a phytopathogen *Ralstonia pseudosolanacearum*. J Bacteriol
908 207:e0027324.

909 90. Zhang Y, Li J, Zhang W, Shi H, Luo F, Hikichi Y, Shi X, Ohnishi K. 2018. A putative LysR-type
910 transcriptional regulator PrhO positively regulates the type III secretion system and contributes to
911 the virulence of *Ralstonia solanacearum*. Mol Plant Pathol 19:1808–1819.

912 91. Huang J, Wang R, Zhang Q, Wang C, Liang T, Hikichi Y, Ohnishi K, Jiang G, Guo T, Zhang Y.
913 2024. Positive regulation of the PhcB neighbouring regulator PrhX on expression of the type III
914 secretion system and pathogenesis in *Ralstonia solanacearum*. Mol Plant Pathol 25:e13398.

915 92. Marenda M, Brito B, Callard D, Genin S, Barberis P, Boucher C, Arlat M. 1998. PrhA controls a
916 novel regulatory pathway required for the specific induction of *Ralstonia solanacearum hrp* genes
917 in the presence of plant cells. Mol Microbiol 27:437–453.

918 93. Brito B, Marenda M, Barberis P, Boucher C, Genin S. 1999. prhJ and hrpG, two new components
919 of the plant signal-dependent regulatory cascade controlled by PrhA in *Ralstonia solanacearum*.
920 Mol Microbiol 31:237–251.

921 94. Peyraud R, Cottret L, Marmiesse L, Gouzy J, Genin S. 2016. A resource allocation trade-off
922 between virulence and proliferation drives metabolic versatility in the plant pathogen *Ralstonia*
923 *solanacearum*. PLoS Pathog 12:e1005939.

924 95. Minh Tran T, MacIntyre A, Khokhani D, Hawes M, Allen C. 2016. Extracellular DNases of
925 *Ralstonia solanacearum* modulate biofilms and facilitate bacterial wilt virulence. Environ
926 Microbiol 18:4103–4117.

927 96. Perrier A, Barberis P, Genin S. 2018. Introduction of genetic material in *Ralstonia solanacearum*
928 through natural transformation and conjugation. Methods Mol Biol 1734:201–207.

929 97. Khokhani D, Tran TM, Lowe-Power TM, Allen C. 2018. Plant Assays for Quantifying *Ralstonia*
930 *solanacearum* Virulence. Bio Protoc 8:e3028.

931 98. Lowe-Power TM, Hendrich CG, von Roepenack-Lahaye E, Li B, Wu D, Mitra R, Dalsing BL,
932 Ricca P, Naidoo J, Cook D, Jancewicz A, Masson P, Thomma B, Lahaye T, Michael AJ, Allen C.
933 2018. Metabolomics of tomato xylem sap during bacterial wilt reveals *Ralstonia solanacearum*
934 produces abundant putrescine, a metabolite that accelerates wilt disease. Environ Microbiol
935 20:1330–1349.

936 99. Arora NK, Verma M. 2017. Modified microplate method for rapid and efficient estimation of
937 siderophore produced by bacteria. 3 Biotech 7:381.

938 100. Schwyn B, Neilands JB. 1987. Universal chemical assay for the detection and determination of
939 siderophores. Anal Biochem 160:47–56.

940 101. Chen I-MA, Chu K, Palaniappan K, Ratner A, Huang J, Huntemann M, Hajek P, Ritter SJ, Webb
941 C, Wu D, Varghese NJ, Reddy TBK, Mukherjee S, Ovchinnikova G, Nolan M, Seshadri R, Roux S,
942 Visel A, Woyke T, Eloe-Fadrosh EA, Kyrpides NC, Ivanova NN. 2022. The IMG/M data
943 management and analysis system v.7: content updates and new features. Nucleic Acids Res
944 https://doi.org/10.1093/nar/gkac976.

945 102. Waterhouse AM, Procter JB, Martin DMA, Clamp M, Barton GJ. 2009. Jalview Version 2--a
946 multiple sequence alignment editor and analysis workbench. Bioinformatics 25:1189–1191.

947 103. Sievers F, Wilm A, Dineen D, Gibson TJ, Karplus K, Li W, Lopez R, McWilliam H, Remmert
948 M, Söding J, Thompson JD, Higgins DG. 2011. Fast, scalable generation of high-quality protein
949 multiple sequence alignments using Clustal Omega. Mol Syst Biol 7:539.

950 104. Goujon M, McWilliam H, Li W, Valentin F, Squizzato S, Paern J, Lopez R. 2010. A new

951 bioinformatics analysis tools framework at EMBL-EBI. Nucleic Acids Res 38:W695–9.

952